

## A SPECTRAL ANALYSIS OF THE MASUDA FLARE USING *YOHKOH* HARD X-RAY TELESCOPE PIXON RECONSTRUCTION

DAVID ALEXANDER AND THOMAS R. METCALF

Lockheed Martin Advanced Technology Center, Department H1-12 B252, 3251 Hanover Street, Palo Alto, CA 94304

Received 1996 December 17; accepted 1997 June 13

### ABSTRACT

Masuda's discovery of a compact hard X-ray impulsive source at the apex of a flaring coronal loop has received a great deal of recent attention in the solar physics community. The Masuda flare, which occurred on 1992 January 13, exhibited evidence of energy deposition in a compact region some distance above the soft X-ray loop, suggesting, to some authors, a flare process similar to the classical model for two-ribbon flares proposed by Shibata et al. These conclusions were made on the basis of a maximum entropy method (MEM) reconstruction of the *Yohkoh* Hard X-Ray Telescope (HXT) observations. Recently, a new approach has been developed for reconstructing the spatial information from the HXT: that of pixon reconstruction, proposed by Metcalf et al.

In this paper, we apply the pixon reconstruction technique to the event of 1992 January 13 and determine the temporal and spectral characteristics of the loop-top source. While our emphasis here is on the spectral properties of the Masuda flare, we also provide a brief comparison between the pixon reconstruction and that of MEM for the hard X-ray loop top. In carrying out the comparison between the methods, we have applied recent improvements to the instrument response functions and reconstruction algorithms. We have also identified a previously unknown effect of weak source suppression that was inherent in previous analyses and that significantly compromised the ability to study weak sources of hard X-ray emission in the presence of strong sources. The improved response functions and the better flux estimation used in this paper reduce (but do not eliminate) the effects of this suppression, and consequently, it should be noted that the MEM analysis presented in this paper is quite distinct from any that have been carried out previously.

Our conclusions are that (a) a compact loop-top hard X-ray source exists with an impulsive temporal profile spanning the peak of the flare; (b) the loop-top source is nonthermal in nature at the peak of the flare; (c) there is a distinct dearth of HXT LO channel emission, relative to the higher energy channels, from the loop-top region, indicating either a very hard spectrum or the presence of a low-energy cutoff in the energetic electron spectrum; (d) the footpoint and loop-top emission during the impulsive phase of the flare are produced by two distinct particle populations; (e) following the main phase of this flare, the loop top is clearly thermal in nature with a peak temperature of  $\sim 40$  MK that decreases with time as the event proceeds; and (f) the disparity between the present pixon results and previous MEM results is primarily due to the intrinsically better photometry achieved by the pixon method and the avoidance of suppression effects in the present analysis. These conclusions therefore support, in part, those made in previous works, confirming the existence of an impulsive source of hard X-rays in the corona above a flaring loop. Our analysis does, however, allow for a more comprehensive understanding of the temporal and spectral development of this event in the context of an alternative reconstruction technique.

*Subject headings:* Sun: corona — Sun: flares — Sun: X-rays, gamma rays

### 1. INTRODUCTION

The acceleration of energetic particles is important in understanding the energy release process in solar flares. The interaction of these accelerated particles with the solar atmosphere produces an array of observational signatures from the chromosphere and corona. In particular, the detection and analysis of hard X-ray emission in flares has led to a greater understanding of the type of particles produced in the energy release process and, with the assumption of various photon production scenarios, has yielded information about the energy distribution and flux of the accelerated particles. The latter properties are crucial in constraining any model of particle acceleration in the solar atmosphere. Instrumentation on board the *Yohkoh* spacecraft has added a new dimension to the study of solar flares. The Hard X-Ray Telescope (HXT) provides not only spectral, temporal, and flux information but also spatial information, allowing us to study in detail the sites where the energetic particles deposit their energy (Kosugi et al. 1991).

A surprising discovery from the HXT was the detection of impulsive hard X-ray emission above the coronal portion of flaring loops (Masuda 1994; Masuda et al. 1994, 1995). The results of Masuda et al. (1994) for one particular flare, occurring on 1992 January 13, indicate a compact impulsive source high in the corona with a time profile similar to that of the hard X-ray footpoints. The presence of such a source has led several authors to develop a variety of explanations for this enigmatic and exciting observation.

One of the simplest explanations proposed is that the ambient flare loop presents a thick-thin-thick target to the accelerated electrons, presumed to produce the observed hard X-ray emission via the bremsstrahlung process (Wheatland & Melrose 1995). The justification for treating the upper coronal portion of the loop as a thick target to high-energy electrons ( $> 10$  keV) is based on an assumption that flare loop tops contain a significant amount of high-density plasma ( $\approx 10^{12}$  cm $^{-3}$ ) confined to relatively small volumes (low filling factor). This notion is borne out by the

results of Phillips et al. (1996) from their spectroscopic analysis of several flares seen by the *Solar Maximum Mission* Bragg Crystal Spectrometer (SMM/BCS). To characterize the physical parameters of this high-density region, Wheatland & Melrose (1995) used the results of Feldman et al. (1994), who also argue for high-density flare loop tops from an analysis of *Yohkoh* Soft X-Ray Telescope (SXT) observations of several flares. However, it should be pointed out that while this simple model has some strengths, there is no direct spectroscopic evidence for high density associated with the event of 1992 January 13, nor are there any indications from the SXT that the necessary high densities exist in the soft X-ray emitting plasma. The result of Masuda et al. (1994) that the hard X-ray loop-top source lies above and is distinct from the soft X-ray loop is not accounted for in the Wheatland & Melrose model.

Another relatively simple approach to explaining the Masuda event is that of trapping particles in the region near the apex of the loop. This explanation has been broached by several authors, but the most comprehensive study has been carried out by Fletcher (1995), who uses a stochastic simulation of electron transport to derive the bremsstrahlung photon production from a distribution of energetic electrons injected at the loop apex. The trapping in this model results from an imposed convergence of the magnetic field in the upper layers of the chromosphere. The resulting loss cone, combined with the collisional pitch angle scattering of the particles, serves to govern the transport properties of the injected electrons. The key factor to producing hard X-ray photons at the loop apex is the existence of electrons injected with large pitch angles ( $\mu = \cos \theta \approx 0$ ). Fletcher (1995) chose an injected electron distribution that was isotropic in pitch angle cosine. This results in a significant number of electrons at large enough pitch angles to produce an impulsive loop-top hard X-ray source of the type reported by Masuda (1994). No detailed temporal comparison with the HXT results was done by Fletcher (1995), who integrated over the particle lifetime and restricted her considerations to the case of impulsive particle injection. Consequently, the results from this work are strictly only appropriate for the first few seconds (a typical electron lifetime) of the flare. This problem can be circumvented, however, by the inclusion of a time-dependent source function for the electron injection (e.g., MacKinnon 1988). In addition, no direct comparison between the observed HXT flux and the expected bremsstrahlung flux was carried out. It is not clear from this work that electrons with large pitch angles will remain at or near the loop top for a long enough period nor that there are enough of these electrons to explain the observed time behavior and flux of the observed emission. Specifically, the pitch angle scattering rate is significant, and, consequently, an electron with an initial pitch angle of  $90^\circ$  will rapidly scatter to smaller pitch angles and be carried away from the loop top. The spectral properties of the X-ray emission resulting from this approach indicate footpoints consistent with thick-target bremsstrahlung photon production and a loop top that is predominantly thin-target emission (although not entirely), in agreement with the observed behavior (see Fletcher 1996 and Wheatland & Melrose 1995). The model proposed by Fletcher (1995) is thus very attractive and worth further development.

Takakura et al. (1993) have shown that coronal hard X-ray emission, as observed in four impulsive flares includ-

ing the Masuda event, has a temporal behavior indicating a hard X-ray brightening that begins at the top of a single coronal loop and then spreads throughout the loop during the flare rise phase, with a speed of order  $10^4 \text{ km s}^{-1}$ . It is argued that this behavior is consistent with the idea that anomalous heat conduction is responsible for triggering the onset and early phase of hard X-ray bursts (Takakura 1992). The enhanced heating in this model is due to the dissipation of field-aligned electric currents by an anomalous resistivity that is in turn caused by electron plasma waves excited by an enhanced heat conduction at the loop top during the flare initiation.

All of the studies discussed above assume that the loop-top source lies inside a single magnetic flux tube or loop. However, a comparison with the soft X-ray emission for the flare of 1992 January 13 (Masuda 1994) shows that the localized hard X-ray source near the loop top is, actually, spatially distinct from the loop defined by the soft X-ray emission. This adds a degree of complexity that makes this event particularly intriguing. A model has been presented by Masuda and colleagues (e.g., Shibata et al. 1995; Tsuneta et al. 1997) to explain this exciting discovery. In this model, a reconnection jet produced high above the loop impinges on the loop top, creating a fast-mode MHD shock, super-hot plasma, and possibly high-energy electrons. The super-hot plasma is then responsible for the hard X-ray emission through the process of thermal bremsstrahlung. It is not clear to the present authors how the scenario proposed by Masuda (1994), Shibata et al. (1995), and Tsuneta et al. (1997) can explain all the facets of this event. In particular, it is not made evident how the soft X-ray loop is formed in one flux tube by the injection of energy into a different flux tube.

It has been argued that the formation of the soft X-ray loop is delayed in time by the requirement that the loop fill with dense, hot plasma (Aschwanden et al. 1996). A typical hydrodynamic timescale for this process is 30–60 s. During this time, the reconnection region progresses to higher altitudes, causing an apparent separation between the particle production (the loop-top source) and their effects on the ambient atmosphere (the soft X-ray loop). This argument is appealing. However, an analysis of the soft X-ray observations shows only a relatively modest increase in the loop height over the duration of the event; at no time is the magnetic flux tube that connects the hard X-ray loop-top source to the surface ever hot or dense enough to yield significant fluxes in the SXT. The relationship between the dynamics of the acceleration site and that of the resulting soft X-ray loops (e.g., chromospheric evaporation) is likely to be quite complicated and should be studied further (cf. Forbes & Acton 1996). In the case of the Masuda event, however, the basic difficulty still remains that the field lines connecting the presumed acceleration site (loop-top source) with the footpoints do not show any evidence for a significant hydrodynamic response, for which there should be a soft X-ray signature.

Masuda (1994) concluded that the impulsive coronal source had a time profile similar to that displayed by the footpoints. In his model the coronal source is presumed to be generated in situ by thermal bremsstrahlung from a localized superhot plasma, while the footpoint emission results from the interaction of energetic particles with the ambient chromosphere. It is not clear in this scenario why these two distinct emission processes would yield identical

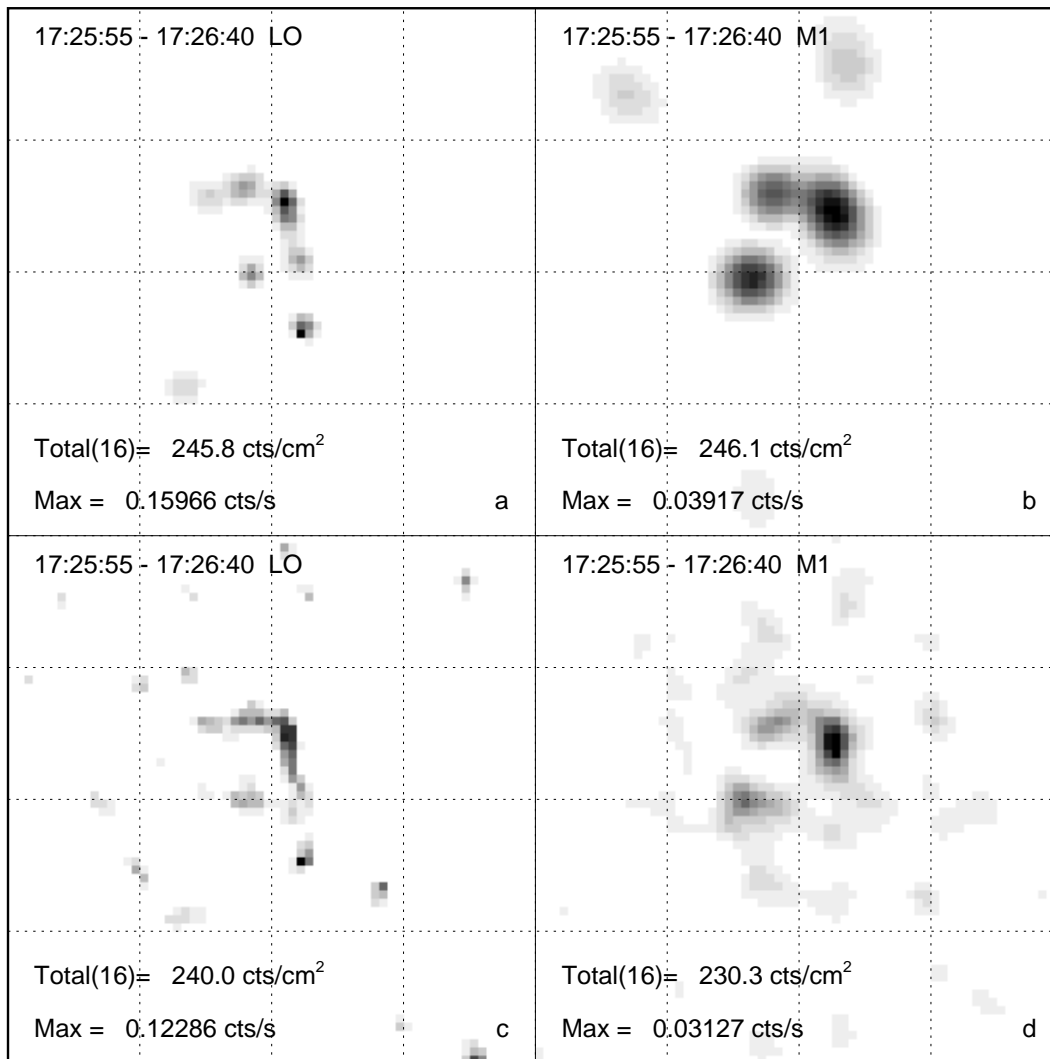


FIG. 1.—Comparison of pixion and MEM calculations for the LO and M1 channels. Reconstructed HXT images for the LO and M1 channels produced with pixions are shown in (a) and (b), while the corresponding MEM maps are shown in (c) and (d). Each image is independently scaled, with the maximum value indicated on the figures. The images are negatives with solar north up and solar east to the left. The images are  $64 \times 64$  pixels with a  $2.5$  pixel size.

time profiles over the duration of the impulsive phase (some 60 s in Masuda 1994, although see Figs. 3 and 5 of this paper). Ryan & Hudson (1995) have estimated that the electron thermalization time for Coulomb collisions is on the order of  $\tau_{ee} = (6 \times 10^{-3}) T_e^{3/2} n_e^{-1}$  s, where  $T_e$  and  $n_e$  are the electron temperature and number density, respectively. For temperatures and densities required to explain the observed loop-top emission in the 1992 January 13 flare, the thermalization time is 56 s. The time variability of the loop-top source is much shorter than this thermalization time, indicating a serious difficulty for a thermal source interpretation.

Whatever the explanation for the Masuda event, Tsuneta (1996) and others have made the assertion that the detection of nonthermal hard X-ray emission at flare loop tops provides a strong indication that magnetic reconnection is the predominant mechanism by which energy is released in a solar flare. This is corroborated, to some degree, by the work of Aschwanden et al. (1996), who associate the location of the coronal emission with the particle acceleration site using a time-of-flight analysis on hard X-ray data from BATSE.

All of the work described above relies on the various facets of the observed hard X-ray emission and, in particular, its spatial information. In devising their models, the authors have depended heavily on the reported results of Masuda et al. (1994). In this paper, we apply an alternative analysis technique to this singularly important event and reach some definitive conclusions regarding the possible spectral properties of the particles responsible for this emission. The hard X-ray observations of the event are described in § 2. Our reconstruction technique and its relationship to that of Masuda et al. (1994) is introduced in § 3, with our imaging results being discussed in § 4. Section 5 deals with the differences between the Masuda results and those presented in this paper. The spectral characteristics of the observed emission are determined in § 6, and we relate our description of the Masuda event to the various models and conclude in § 7.

## 2. THE MASUDA EVENT: 1992 JANUARY 13 17:27 UT

As discussed in the Introduction, the flare of 1992 January 13, commonly known as the Masuda event, has generated much interest throughout the solar community,

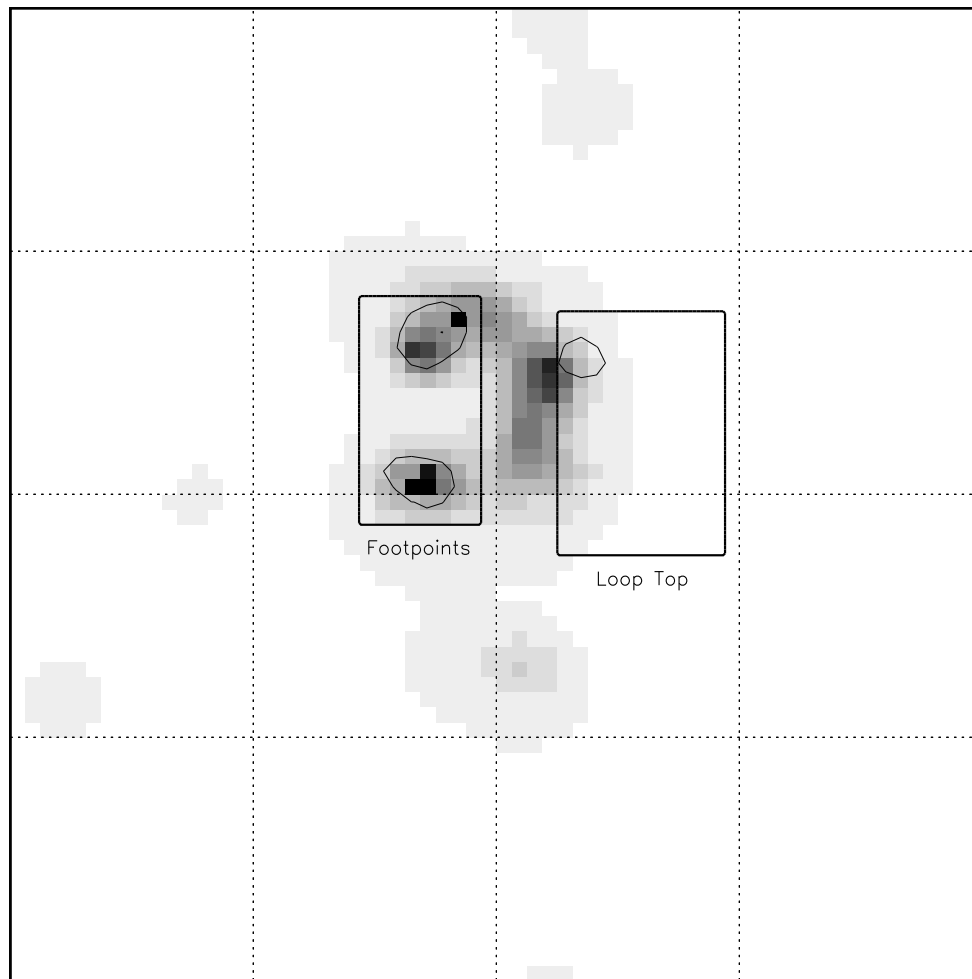


FIG. 2.—An HXT image in the LO channel at 1992 January 13 17:27:40–17:28:20 UT. The image is square-root scaled. The thin contour shows the 7.5% contour of the M1 emission, and the thick contour shows the integration boxes. One box was chosen to enclose both footpoints, while the other was chosen to enclose the loop top. The sizes of the individual boxes were chosen to enclose the bulk of the M1 emission emanating from the enclosed sources.

particularly in the debates over the role of reconnection in solar flares (Tsuneta 1996) and the relative roles of energetic electrons and protons in the flare energy budget (Cargill, Emslie, & Simnett 1996).

The flare of 1992 January 13 was of *GOES* class M2.0 and occurred in active region NOAA 6994 near the west limb of the Sun. No associated  $H\alpha$  emission was seen in the chromosphere, possibly indicating that the loop was partly occulted by the solar limb (Wang et al. 1995). This explanation is somewhat at odds with the hard X-ray observations, which clearly show footpoints that are located predominantly on the eastern side of the west limb (Aschwanden et al. 1996). A partial occultation of at least one of the footpoints should not be precluded, however, since there are some indications from the hard X-rays that this is actually occurring. This is currently under investigation by the present authors.

From an image reconstruction of this event using an MEM inversion of the HXT data, Masuda et al. (1994) demonstrated that the flare loop displayed double footpoint sources in the energy bands above  $\approx 20$  keV, characteristic of many flares seen with the *SMM* hard X-ray imaging spectrometer (Hoynig et al. 1981; Duijveman et al. 1982) and *Hinotori/SXT* (Takakura et al. 1984). The double footpoint nature of solar hard X-ray bursts has been found to be one

of the basic properties of impulsive hard X-ray emission (Sakao 1994).

Masuda et al. (1994) also concluded that this event displayed a *loop-top hard X-ray source*, seen in the M1 and M2 channels of the HXT, corresponding to photon energy ranges 22.7–32.7 keV and 32.7–52.7 keV, respectively. This source was located above the flaring loop seen in soft X-rays. Coronal hard X-ray emission of this sort is not commonly observed. Indeed, Masuda (1994) has identified only six such events in the *Yohkoh* database. It is the detection of these localized sources in the corona that has generated the wealth of interest outlined in the Introduction. For the event of 1992 January 13, the MEM reconstruction and subsequent analysis of the loop-top source by Masuda et al. (1994) led to the conclusions that (a) the hard X-ray coronal source lay some  $10''$  above the corresponding soft X-ray loop, (b) the temporal behavior of this emission in the M1 channel was impulsive and mirrored that of the footpoint emission, (c) the relative intensity of the loop-top source to the combined emission from both footpoints was approximately 20%, and (d) the loop-top emission was thermal with a temperature of 200 MK (LO/M1 ratio) and 130 MK (M2/M1 ratio) and corresponding emission measures of  $5 \times 10^{43} \text{ cm}^{-3}$  and  $9 \times 10^{43} \text{ cm}^{-3}$ . (The LO channel of the HXT spans a photon energy range of 13.9–22.7 keV.) This

last conclusion could be modified if the loop-top emission was generated by a nonthermal distribution of particles. In this case, the spectral index of the photon spectrum detected was 2.6 and 4.1, respectively, for the M1/LO and M2/M1 flux ratios (Masuda 1994).

The conclusions reached by Masuda et al. (1994) for the spectral properties of the loop-top source require some comment. The scenario favored by these authors was that the loop-top source was thermal, resulting from the heating of the localized plasma by a shock front impinging on the closed-loop structure illuminated by the soft X-ray emission. We will show that the observed flux ratios are more consistent with a nonthermal source. In addition, the spectral analyses carried out in previous works have been very limited in that only a single time at the peak of the event has been discussed in detail. However, note that, in his study of eight flares at the limb, Masuda (1994) concluded that "later in the gradual phase all eight flares reveal a 'loop-top' source which is characterized by a steep spectrum ( $T < 40$  MK) and a gradual variation" (p. 26).

Very recently, Tsuneta et al. (1997) analyzed SXT images for the 1992 January 13 flare and succeeded in detecting soft X-rays from the location of the hard X-ray loop-top source. The soft X-ray emission is weak, but, by summing the SXT images, spatially and temporally, they were able to discover a hot source (15–20 MK) coincident in position with the HXT loop-top source. The SXT source evolves during the flare into two ridges, one on either side of the HXT source, suggesting an association with an X-type reconnection region.

The Masuda et al. (1994) results were based on a careful analysis of HXT images from a MEM reconstruction of the data. Recently, however, an alternative reconstruction technique has been applied to the problem of interpreting HXT information (Metcalf et al. 1996).

### 3. THE PIXON RECONSTRUCTION APPROACH

Reconstructing images from data collected by a Fourier imaging instrument such as the HXT requires the use of nonlinear methods to obtain the best results. A maximum entropy technique was first successfully applied in X-ray imaging astronomy by Willingale (1981) for the analysis of *Einstein* data. A similar technique was later developed for use with rotating modulation collimator data from the *Hinotori* satellite (Tsuneta 1984). More recently, an MEM approach has been utilized in the analysis of solar flare data from the HXT (Sakao 1994; Masuda 1994; see above), while a pixon-based reconstruction approach has been developed by Metcalf et al. (1996). It is this pixon approach that we will apply to the Masuda event in this paper.

Both the pixon and the MEM approaches apply the Bayesian method of logical inference (see Loredo 1990) to reconstruct an image from the noisy and sparse HXT data. The pixon approach is also a maximum entropy method but with the refinement that it allows for a variable pixel (or *pixon*) size. These nonlinear techniques, therefore, share much in common. A key difference between them lies in how they deal with the number of degrees of freedom. This is particularly important when the data are sparse. While MEM assumes no correlation between the individual pixels and therefore has as many as  $64 \times 64$  dof (the typical size of an image), the pixon approach minimizes the dof by creating a *pixon map* where the individual pixon sizes vary to accommodate the information content in the data (the more

information at a given location, the smaller the pixon size there). For a typical HXT image, the number of degrees of freedom in the pixon approach is  $\sim 100$ , comparable to the number of data points. Despite the commonality between these methods, we have chosen to use the terminology MEM to refer to the standard maximum entropy approach and to distinguish this from the pixon method. In using the pixon method on an instrument like the HXT, it turns out that the entropy term is not critical for the production of reconstructed images that have a good fit to the data (Metcalf et al. 1996).

One of the basic improvements that the pixon approach makes over the MEM approach is better photometry (Metcalf, Alexander, & Kosugi 1997). This is illustrated in Figure 1, which shows a comparison between the pixon and the MEM approach, for a single reconstructed image from the event of 1992 January 13. The photometry disparity between the methods can be alleviated to some degree by choosing large integration times (see Fig. 5 below) and/or large integration boxes, either of which increases the signal-to-noise level. However, for studying the detailed temporal development of a localized weak source, we believe that the present pixon approach has a distinct advantage over the MEM approach.

Since the original submission of this manuscript, a workshop focusing on the reconstruction of HXT images was held at Lockheed Martin Advanced Technology Center (Alexander 1997). One of the major results of this workshop was the implementation of new HXT instrument response functions derived from in-orbit calibrations for the LO and M1 channels of the HXT (Sato 1997). All images and corresponding analyses of data from these two channels appearing in this paper incorporate these new calibrations. In addition, the analysis of pseudodata at the HXT workshop identified a misestimation of the detected flux that was inherent to both the pixon and MEM reconstruction algorithms (this misestimation corresponded to a systematic error in the determination of the DC offset in the collimator responses; see Kosugi et al. 1991). This analysis is currently being prepared for publication (Metcalf et al. 1997). All pixon reconstructions used in this paper have been generated using the algorithms corrected for this misestimation. A corresponding correction has also been made to the

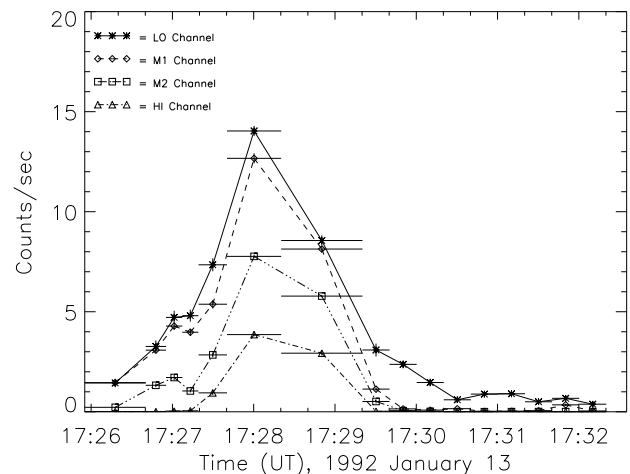


FIG. 3.—Light curves for the LO, M1, and M2 channels of the HXT for the footpoint regions depicted in Fig. 2. The horizontal error bars indicate the accumulation time used for each point.

MEM reconstructions used for comparison purposes in this paper (except where otherwise stated).

It is evident from Figure 1 that in the pixon reconstructions most of the emission is concentrated in the strongest sources and is less dispersed throughout the field of view. The effects of this will be discussed in more detail below. In both methods, it should be noted that the emission shown is regarded as being statistically significant by the algorithm used and is, therefore, consistent with the data. We regard the lack of spurious sources in the pixon approach to be a distinct advantage over MEM.

For a detailed description of the pixon technique, the reader is referred to Piña & Puetter (1993), Puetter (1995), and Metcalf et al. (1996).

#### 4. TEMPORAL VARIATION OF THE HARD X-RAY EMISSION

To study the dynamical nature of the hard X-ray emission in the event of 1992 January 13, we consider two separate spatial regions of the flaring structure. One region encompasses both footpoints and represents the total radiation resulting from the electrons that precipitate to the chromosphere. The other region is that of the loop top, which allows us to investigate the nature of the coronal emission. These regions are displayed in Figure 2. The image shown was generated using the pixon approach described above. Figure 2 clearly shows the loop structure seen in the HXT LO channel. The box identified as the loop-top region was chosen to incorporate all the loop-top M1 emission but to exclude as much of the loop as possible. As long as this limited overlap with the loop is maintained, it is found that changing the box size has little effect on our results.

Having isolated the regions of interest, we can investigate their temporal behavior independently. Figures 3 and 4 show the light curves for each of the chosen regions in each of the HXT channels. There are significant counts in the HI channel (53–100 keV) for the footpoints but not for the loop top, so we have chosen not to show this channel in Figure 4. The footpoint images in the HI channel do show a very clear nonthermal impulsive signature similar to that seen in the lower energy channels. Figures 3 and 4 show that the principal flaring stage of this event displays impulsive footpoints in all channels, a loop-top source in the HXT/LO

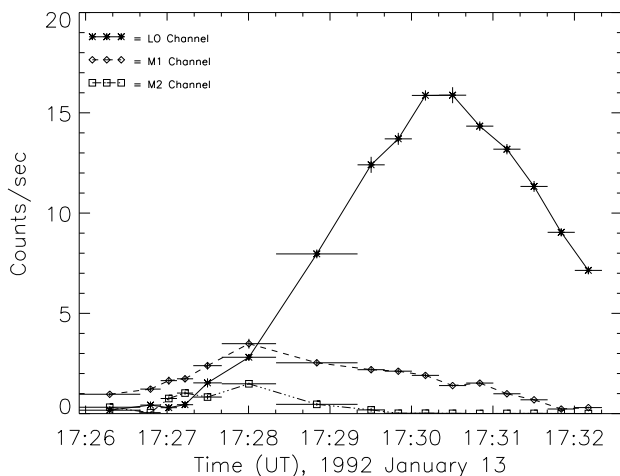


FIG. 4.—Light curves for the LO, M1, M2, and HI channels of the HXT for the loop-top region depicted in Fig. 2. The horizontal error bars indicate the accumulation time used for each point.

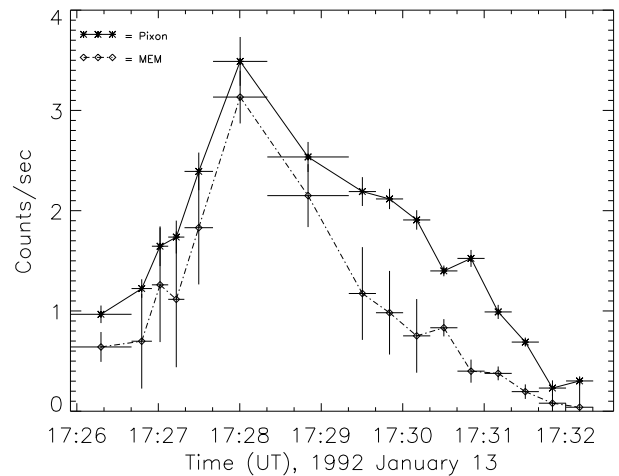


FIG. 5.—Comparison of HXT image photometry resulting from MEM and pixon reconstructions for the loop top using the HXT M1 channel.

channel that increases to a peak before decaying gradually to preflare levels, a loop-top source in the M1 channel which is impulsive around the peak of the flare and gradually decaying thereafter, and a very weak loop-top source in the M2 channel that is impulsive in nature. We also see that for the loop top there is a distinct lack of LO channel emission during the flare peak. This will be discussed below.

In Figure 5 we present a comparison of the pixon and MEM reconstructions for the M1 loop-top source for the flare of 1992 January 13. With the exception of the decay phase of the loop-top source, the time profiles are remarkably similar. The horizontal error bars indicate the accumulation time for a given image, while the vertical error bars represent the range of statistically allowed ( $1\sigma$ ) count rates for the particular reconstruction shown. The vertical error bars do not show the range of count rates that could be present for different reconstructions. Hence, the vertical error bars do not give any meaningful measure on how well the reconstructed images represent the “true” distribution of emission. The level of agreement between the two techniques gives us some confidence that the light curves shown are a fair representation of the true temporal variation of the source. A more quantitative statement regarding the accuracy of the reconstructed images requires a detailed analysis of pseudodata covering a range of test cases. Such a detailed study is underway (Metcalf et al. 1997), with some preliminary results being discussed briefly by Alexander (1997). It is important to emphasize here that the MEM results presented in Figure 5 incorporate corrections for the newly calibrated modulation patterns, for the inaccuracies in the flux-estimation, and for the effects of weak source suppression. Consequently, the MEM light curve shown is not representative of previous MEM analyses (e.g., Masuda 1994).

During the principal phase of this event, it is evident from Figures 3 and 4 that the hard X-ray footpoints are impulsive. This behavior is apparent in all the HXT channels and is a standard characteristic of solar flares (Hoyng et al. 1981). Indeed, Sakao (1994) has shown that for this flare, and many others, the footpoints brighten simultaneously in the M2 band of HXT (33–53 keV), to within 0.5 s, consistent with the idea that the acceleration region is at a location that is equidistant from either footpoint. The duration of the impulsive energy injection for the flare being studied

here varies with energy, but we note that the rise time for the footpoints is  $\sim 60$  s for all channels.

The gradual buildup of thermal emission in the loop-top region is clearly displayed by the LO channel (14–23 keV; Fig. 4), which can be regarded as a reasonable proxy for the soft X-ray emission. Via the LO channel light curves we see that the loop-top intensity grows as the event proceeds. This is consistent with the hydrodynamic modeling of the atmospheric response to impulsive energy input (Mariska, Emslie, & Li 1989) whereby the density and temperature of the loop-top slowly increases throughout the rise phase of the flare. This would indicate that the LO channel is seeing primarily thermal emission at least late in the event. The M1 channel (23–33 keV) emission from the loop-top region (Fig. 4) demonstrates a significantly different light curve in which a relatively rapid rise and initial decay is followed by a distinctly more gradual decay phase. A comparison of the loop-top emission with that of the combined footpoint emission shows that the loop top attains a relatively strong peak of some 30% of the peak strength of the footpoints.

The behavior displayed by the loop-top source in the present work is substantially different from that determined from previous analyses that have relied entirely on MEM reconstructions and that were unaware of the effects of suppression. The impulsive nature of the emission high in the corona seen during the peak of the event is only part of the overall picture. The light curve here is complicated by the intermingling of nonthermal and thermal emission (see later). This was not fully realized by previous authors because of two main photometric effects prevalent in the MEM reconstructions. First, the MEM approach suffers from the generation of spurious sources, at some level, which reduce the statistical significance of any weak true sources, especially outside the time of the flare peak. Second, the coexistence of very bright (footpoints) and very weak (loop top) sources in the same field of view, combined with the relatively short integration times used by Masuda (1994), result in a suppression of the loop-top signal. This is discussed more fully in the next section. The result of these two effects in the Masuda analysis is an MEM loop-top source that displays very short rise and decay times.

The impulsive behavior of the loop-top source is most clearly seen in the M2 channel (33–53 keV). However, given our integration times (chosen to be equal in all channels to facilitate the spectral analysis), the temporal information obtained from the M2 channel is limited. This was acknowledged by Masuda (1997), who used a Gaussian fitting technique to improve on the time resolution of the loop-top source in the M2 channel. With this approach, Masuda (1997) determined that in this energy channel the loop-top emission peaks some 5–10 s prior to similar emission from the footpoints. For the present analysis we are limited to the results shown in Figure 4.

The detailed description of the impulsive loop top presented here is an addition to and a clarification of previous studies of this flare. In particular, we discuss the association between the loop top and the footpoint emissions, which has severe implications for many of the models discussed in the Introduction. One thing to note is that the curves in Figures 3 and 4 were produced using a variable accumulation time. In particular, an accumulation time during the peak of the event was chosen to be quite long,  $\simeq 40$  s. This was done to counteract the signal suppression that occurs in the reconstruction techniques (both MEM and pixon)

when there is a weak source (e.g., the loop top) in the presence of a very strong source (e.g., the footpoints). This is an important point in understanding the principal differences between the MEM and pixon calculations and will be discussed in detail in the following section.

#### 5. FOURIER SYNTHESIS IMAGING: PHOTOMETRIC CONSIDERATIONS

The nature of the HXT data ensures that any valid reconstruction, regardless of the algorithm (MEM, pixon, or any other methods), will have the same number of total counts within the field of view. The reconstruction problem can be posed as

$$f_i = \iint I(x, y)M_i(x, y)dx dy, \quad (1)$$

where  $f_i$  is the measured flux in subcollimator  $i$ ,  $I(x, y)$  is the image we are trying to reconstruct, and  $M_i(x, y)$  is the modulation pattern for subcollimator  $i$ . If we make a linear superposition of the equations in (1), we have

$$\sum_{i=1}^N c_i f_i = \sum_{i=1}^N c_i \iint I(x, y)M_i(x, y)dx dy \quad (2)$$

or, equivalently,

$$\sum_{i=1}^N c_i f_i = \iint I(x, y) \sum_{i=1}^N c_i M_i(x, y)dx dy, \quad (3)$$

where the  $c_i$  are arbitrary constants. If we can find a set of constants such that

$$\sum_{i=1}^N c_i M_i(x, y) \equiv 1, \quad (4)$$

for all  $x$  and  $y$ , then

$$\sum_{i=1}^N c_i f_i = \text{constant} = \iint I(x, y)dx dy. \quad (5)$$

Thus, provided that the modulation patterns are sufficiently diverse to satisfy condition (4), the total number of counts in the reconstructed image must be identical for any valid (i.e., statistically correct) reconstruction. This condition holds approximately for the HXT modulation patterns. Employing the newly calibrated response functions (Sato 1997), we have estimated that condition (4) is correct to  $\approx 4\%$  or better; i.e.,  $c_i$  can be found such that  $\sum c_i M_i$  is within 4% of unity for the majority of the pixels.

As a consequence, since both the MEM and the pixon reconstructions give adequate fits to the subcollimator data, both reconstructions must have the same total counts in the field of view. It is clear, however (see Fig. 1), that the MEM reconstructions are more prone to spurious, low-level sources than the pixon reconstructions. This is to be expected since the MEM reconstruction has many more degrees of freedom (up to 4096 for a  $64 \times 64$  image) than the pixon reconstruction (typically 10–100). Now, since equation (5) specifies the total counts in the reconstructed image, the spurious counts in the MEM reconstruction must reduce the counts in the true sources. Consequently, as shown in Figure 5, the MEM photometry of true sources suffers in the presence of spurious sources to varying degrees depending on the strength of the signal and the integration times used.

This effect is most pronounced in the late phase of the 1992 January 13 flare. In the MEM reconstructions, the flux

in the loop-top source is seen to decay rapidly after the main peak of the event. This gives the MEM loop-top source the appearance of being a simple impulsive process, with the light curve mimicking that of the footpoints. However, the behavior of the loop-top source is somewhat different when analyzed using a pixon reconstruction. The pixon reconstruction shows a loop-top source that remains bright well after the impulsive phase. This difference in the MEM and pixon light curves is caused by the generation of spurious sources by the MEM reconstruction late in the event that serve to “steal” counts from the true source. In addition, the production of a low-level uniform background across the whole field of view, inherent to the MEM technique, becomes a bigger problem as the signal strength decreases. Thus, in the decay phase of the loop-top emission, the presence of spurious sources and a low-level background in the MEM reconstructions result in an HXT light curve that is more sharply peaked in appearance, whereas it can be seen from the pixon reconstruction that the loop-top source is more gradually varying after the flare peak.

Another effect present in the HXT reconstructions for the 1992 January 13 event is that of suppression. At the peak of the event, the footpoint sources are considerably brighter than the loop-top source. Since the data obtained by each subcollimator represents the flux in the entire field of view, weighted by the modulation patterns (eq. [1]), the footpoint emission swamps the loop-top emission, even though they are well separated spatially. Hence, at the peak of the event, the loop-top source is not statistically significant compared with the bright footpoint emission, and the algorithms, both MEM and pixon, suppress the loop-top source. This problem can be circumvented by using longer time integrations around the time of the peak footpoint emission (Metcalf et al. 1997). Figure 6 shows an example of the “statistical suppression” of the loop-top source using the pixon algorithm. In this figure, we used a short time integration, and the statistical suppression of the loop-top source during the time of maximum footpoint emission is clearly evident. The MEM algorithm also suffers from this suppression of the loop-top source. However, the pixon reconstruction does a better job of separating statistically significant and statistically insignificant sources (Metcalf et al. 1997). Here, a *statistically significant* source is one that is required by the data given the noise.

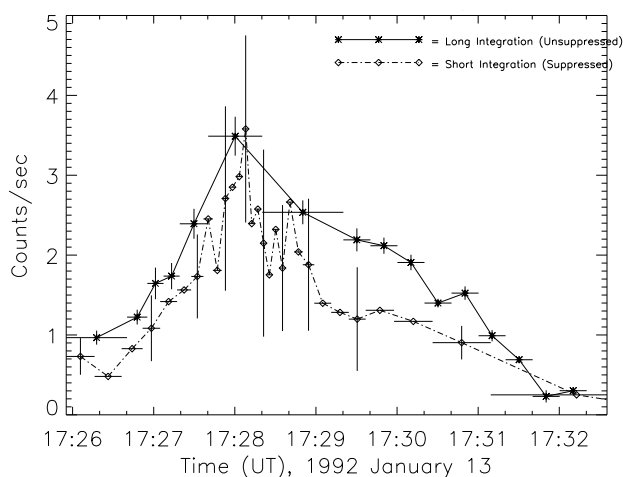


FIG. 6.—The effects of count suppression on weak sources in the presence of strong sources for HXT image reconstruction of M1 channel data.

The effect of this suppression is a new result of the present investigation and was unknown to previous authors. However, it does have an important bearing on the interpretation of previous results. It is clearly important to understand this in the context of the analyses carried out by Masuda (1994) and Masuda et al. (1994). The time profiles, presented in these works, showing a highly impulsive peak for the loop-top source was carried out using an approximate integration time of 8 s per image (Masuda et al., Fig. 2). From the results discussed in this section, it is clear that such a low integration time during the flare peak results in time profiles that are strongly affected by the suppression of the weak loop top by the strong footpoints (see Fig. 6, which shows results for a short integration time of  $\sim 7$  s). The large “impulsive” spike is due to the rising emission from the loop top counteracting the effects of suppression. The consequence of this is that the highly impulsive nature of the loop-top source (approximately 1 minute in duration) resulting from the MEM analysis of Masuda et al. (1994) has to be significantly modified to take account of the effects described here. When this is done, the differences between the MEM and the pixon reconstructions are negligible when the signal-to-noise ratio is relatively high (i.e., during the event peak with large enough integration times); see Figure 5.

In simulations where the correct input is known, the MEM algorithm will often yield a source at the location of a weak, statistically insignificant, “true” source. The statistical significance of this weak source is, however, similar to other spurious sources in the field of view, so that for a real set of observations the validity of the source cannot be confirmed. In the same simulations, the pixon algorithm will completely ignore such a weak source as being statistically insignificant (Metcalf et al. 1997). On the other hand, weak, statistically insignificant, sources that are real would also tend to be ignored by the pixon algorithm. It is clear that when analyzing weak sources in the presence of very strong sources, such as in the 1992 January 13 flare, one must be very cautious since it is intrinsically impossible to determine whether a statistically insignificant source of emission is real or results from noise associated with the strong source.

## 6. SPECTRAL CHARACTERISTICS OF THE HXT EMISSION

In this section we assume that the hard X-ray photons detected in the flare event of 1992 January 13 were produced from a distribution of energetic electrons via the bremsstrahlung process. We will assume both a power-law distribution of injected electrons, acting as a nonthermal tail of a bulk thermal distribution, and a purely thermal distribution of electrons.

The hard X-ray flux,  $I(\epsilon)$  (photons  $\text{cm}^{-2} \text{s}^{-1} \text{keV}^{-1}$ ), observed at the Earth resulting from the injection of energetic electrons with a differential energy spectrum,  $F(E_0) = AE_0^{-\delta}$  (electrons  $\text{cm}^{-2} \text{s}^{-1} \text{keV}^{-1}$ ), is given by

$$I(\epsilon) = a(\delta)\epsilon^{-\delta \pm 1} \quad (6)$$

(see Tandberg-Hanssen & Emslie 1988). This power-law electron distribution represents a suprathermal population of electrons which have energies much larger than the mean thermal energy of the background plasma, an *electron beam*. The exact nature of the photon energy distribution, given in (eq. [6]), depends on the nature of the target plasma with which the energetic electrons interact. The constant  $a(\delta)$  in

equation (6) is a simple function of the electron spectral index,  $\delta$ .

An alternative model for the source of bremsstrahlung photons is that of a hot mass of gas with temperatures sufficiently large that they are able to produce photons at X-ray energies,  $kT \approx \epsilon \approx 10$  keV, i.e.,  $T \approx 10^8$  K. The photon flux resulting from such a particle distribution is

$$I(\epsilon) = D \frac{Q}{\epsilon T^{1/2}} e^{-\epsilon/kT} \tag{7}$$

(Tandberg-Hanssen & Emslie 1988), where  $D$  is a constant and  $Q = n_e^2 V$  is the emission measure of the source that is assumed to be isothermal in this description.

Having generated the photon production, we now calculate how many photons will be detected by the HXT and at what energies. From Kosugi et al. (1991), we have that the photon flux,  $\Phi$  (counts  $\text{cm}^{-2} \text{s}^{-1}$ ), detected by the HXT as photons with energies,  $p_1$  to  $p_2$ , is

$$\Phi = \int_{p_1}^{p_2} \int_0^\infty I(\epsilon) \eta(\epsilon) G(\epsilon, p) [1 - s(\epsilon)] d\epsilon dp, \tag{8}$$

where  $\eta(\epsilon)$  indicates the transmission efficiency of the HXT filter (actually the aluminum casing surrounding the crystals) for the collimators,  $G(\epsilon, p)$  indicates the pulse-height distribution of the detector, and  $s(\epsilon)$  indicates the probability that an incoming photon will escape with an

energy  $\epsilon$ ; this is, the  $K$ -escape of Takakura et al. (1993), where  $s(\epsilon) \equiv f(K)$ .

We are now in a position to calculate the HXT flux for a given electron spectrum at the Sun. In order to determine the relevant spectral parameters, such as spectral index for the power-law cases and temperature for the thermal case, we require flux ratios between the various HXT channels, e.g.,  $\Phi(\text{LO})/\Phi(\text{M1})$ ,  $\Phi(\text{M1})/\Phi(\text{M2})$ ,  $\Phi(\text{M2})/\Phi(\text{HI})$ . This will yield a coarse value for the spectral parameter of interest. Figure 7 shows each of the flux ratios possible using all four channels of the HXT for a range of electron spectra. We can see clearly from Figure 7 that only an extremely hot plasma is able to produce significant count rates in the M1 channel (23–33 keV) and that if this plasma is isothermal, then all flux ratios must yield the same temperature. Figure 7 also demonstrates, quite effectively, the difference between the assumption of a thin or thick target.

Using the results from Figure 7 and the observed values of the flux ratios from the HXT for the loop-top source, we are able to produce the temporal behavior of the best-fit spectral parameters ( $T$ ,  $\delta_{\text{thin}}$ ,  $\delta_{\text{thick}}$ ). This yields some interesting results. Assuming a purely isothermal plasma as the source of the HXT photon fluxes (see eq. [7]), we see from Figure 8 that we are unable to obtain a consistent temperature from the available flux ratios for the loop-top source at the flare peak. Late in the event when we only have LO and M1 emission, we see evidence that the loop top is a pure thermal source with a temperature behavior

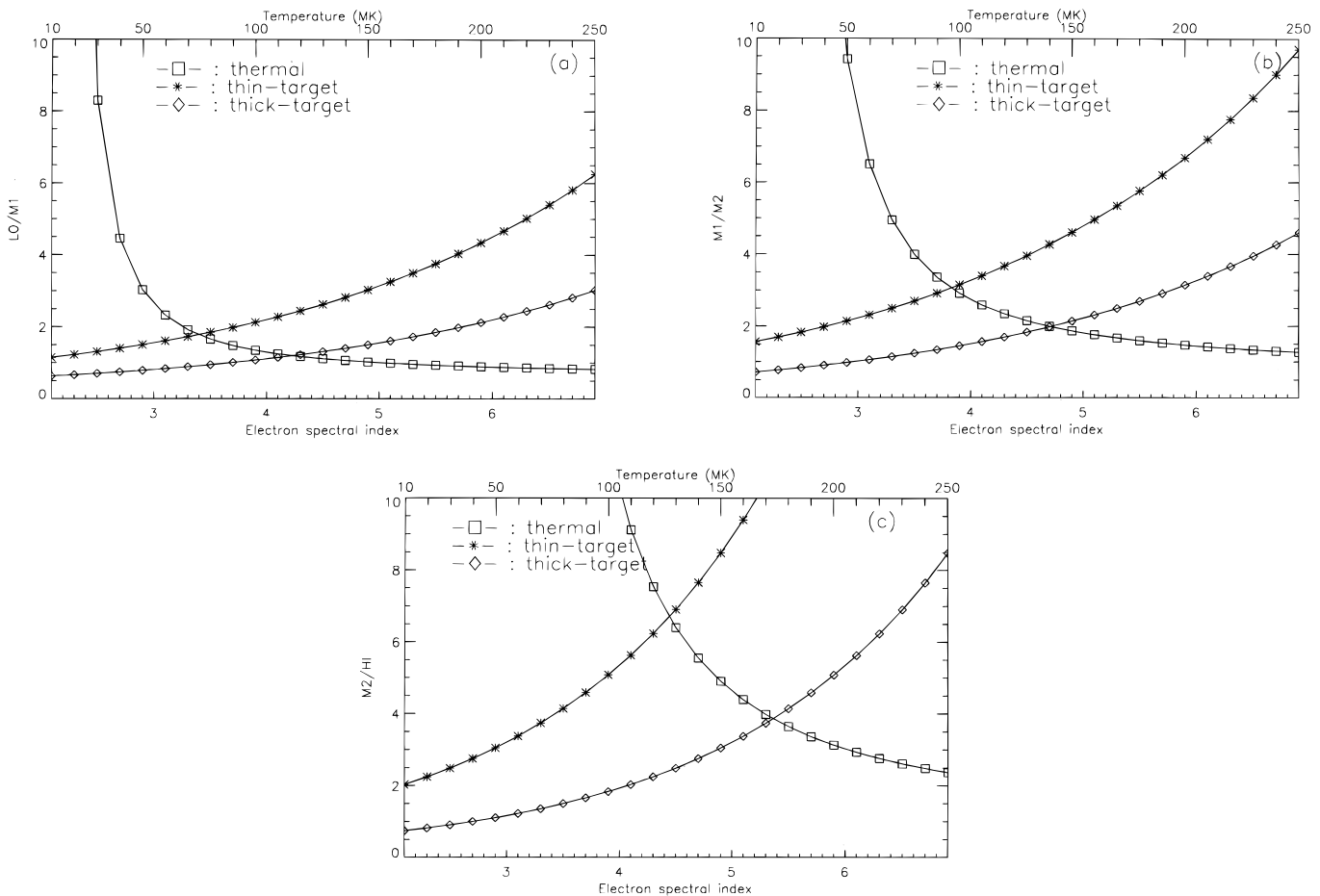


FIG. 7.—HXT channel ratios for different injected energy spectra: (a) LO/M1, (b) M1/M2, and (c) M2/HI

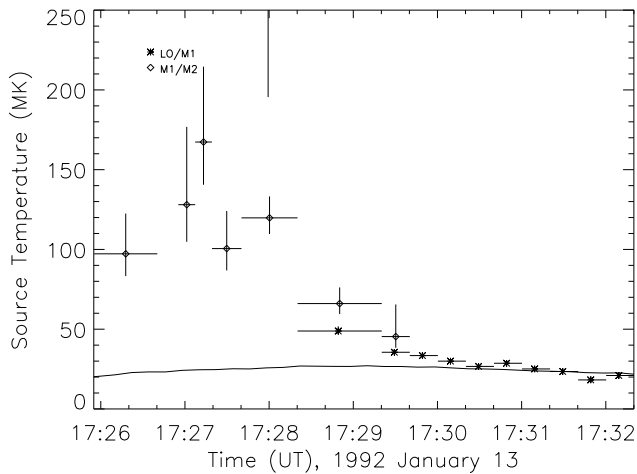


FIG. 8.—Time variation of temperature derived from the various channel ratios, discussed in the text, for the loop-top region. The thin solid line shows the temperature derived from the Fe xxv channel of the *Yohkoh*/BCS.

similar to that displayed by the Fe xxv channel of the BCS, as depicted by the solid line in Figure 8. Prior to this time, it is clear that the loop top cannot be explained by thermal bremsstrahlung from a single isothermal plasma. Our principal justification for this statement is the observation that, even at the peak of the event where there are significant counts in the M2 channel, the available flux ratios yield widely disparate temperatures. This is primarily a result of the dearth of LO channel hard X-ray emission emanating from the loop-top region. The lack of evidence for a thermal source is consistent with the analysis of Ryan & Hudson (1995), who argued that the thermalization time for a plasma with the physical characteristics as determined by Masuda et al. (1994) was too long to explain the observed variability of the loop-top source. Recently, a very interesting paper by Tsuneta et al. (1997) has appeared that discusses in detail the relationship between the hard X-ray loop-top source and the soft X-ray emission as detected by the SXT. It was found that the temperature distribution as determined by the soft X-ray analysis indicated a structure, lying above the main soft X-ray loop, which displayed two high temperature ridges. The hard X-ray loop-top source lies between the soft X-ray temperature humps in a region where the pressure starts to increase. Tsuneta et al. (1997) associate the location of the hard X-ray source with the site of the cooling outflow jet lying in between the slow shocks of a magnetic reconnection site. The hard X-ray source is assumed to be thermal with a temperature of 100–150 MK heated by the fast shock emanating from the reconnection site. These authors state that there is no way to differentiate between thermal and nonthermal models for the loop-top source given the existing data set. This is certainly true when the spectrum is determined using only a single flux ratio. In the present work we have used all three energy channels in which the loop top is detected to determine a self-consistent temperature with little success. Indeed, for the LO/M1 flux ratio, we determine a temperature of  $> 300$  MK, while for the M1/M2 ratio a value of  $120 \pm 10$  MK is obtained.

Assuming that the parent electron population is in the form of a *single* power law in energy, we can use the HXT data to generate the variation of the electron spectral index,

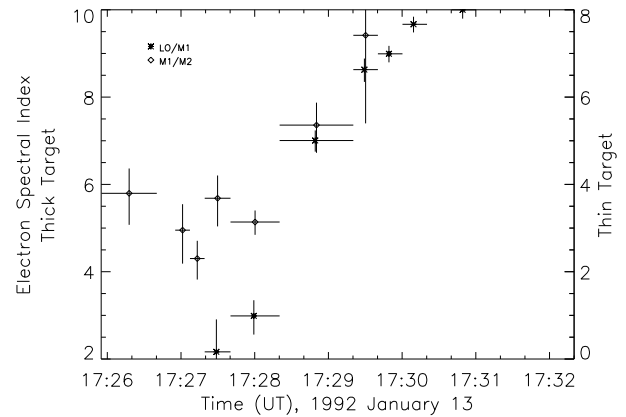


FIG. 9.—Time variation of the electron spectral index derived from the various channel ratios, discussed in the text, for the loop-top region.

$\delta$ , with time. It is clear from the discussion above that the form of the ambient atmosphere, whether it presents a thin or thick target to the incident nonthermal electrons, affects only the value of the spectral index, with  $\delta_{\text{thick}} = \delta_{\text{thin}} + 2$ . There is no way of determining from the data whether the target is thick or thin. However, assuming a direct connection between the hard X-ray loop-top source and that of the footpoints, we can look for a single spectral distribution capable of producing both the footpoint emission and that of the loop top. Prior to 17:27 UT the count statistics were too low to place any confidence in the flux ratios obtained. Later than 17:29 UT we have determined that the loop top is thermal and that there is very little footpoint signal in any but the LO channel.

An examination of the footpoint spectra shown in Figure 10 indicates that all three independent channel ratios yield a single spectral index of  $\delta = 4.1 \pm 0.1$  over the peak of the event (17:27:40–17:29:20 UT) when we assume a thick-target source region. For the case of the loop top we only have reliable M2 channel emission at the peak of the event (17:28:00 UT). We see from Figure 9 that there is a distinct disparity between the spectral index inferred from the LO/M1 flux ratio and that inferred from the M1/M2 flux ratio. The LO/M1 ratio yields a very hard spectral index,  $\delta_{\text{thin}} \approx 1.0$ ,  $\delta_{\text{thick}} \approx 3.0$ , while the M1/M2 ratio yields

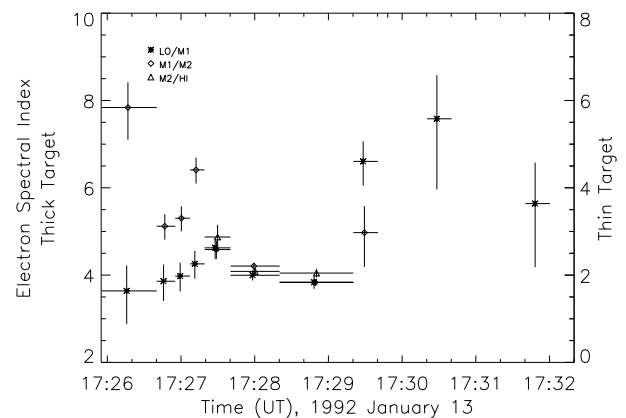


FIG. 10.—Time variation of the electron spectral index derived from the various channel ratios, discussed in the text, for the footpoints.

$\delta_{\text{thin}} \simeq 3.1$ ,  $\delta_{\text{thick}} \simeq 5.1$ . The reason for this disparity is primarily due to the lack of LO channel emission from the loop-top region, as discussed above.

We can reconcile the results from the two flux ratios in two ways. First, the lack of LO channel emission can be readily understood by the inclusion of a low-energy cutoff in the injected electron spectrum. A low-energy cutoff,  $E = E_c$ , results in modified versions of the flux ratio–spectral index curves shown in Figure 7, and we find that for  $E_c = 18.6$  keV both the LO/M1 and M1/M2 flux ratios yield the same inferred spectral index for the loop top of  $\delta_{\text{thin}} = 2.9$  ( $\delta_{\text{thick}} = 4.9$ ). If a single population of accelerated electrons is to be responsible for both the loop-top and the footpoint emission (assuming some direct connectivity between the two regions), then clearly the loop top cannot act as a thick target to all of the energetic electrons. For a pure thin target the electron spectrum emerging from the loop top and impinging on the footpoint regions would have a spectral index of  $\delta = 2.9$  with a low-energy cutoff at  $E = 18.6$  keV. Such a spectrum would result in observed footpoint flux ratios of  $\Phi(\text{LO}/\text{M1}) \simeq 0.5$ ,  $\Phi(\text{M1}/\text{M2}) \simeq 1.0$ , and  $\Phi(\text{M2}/\text{HI}) \simeq 1.1$ , which are clearly not consistent with the actual observed values of 1.1, 1.64, and 2.0, respectively (see Fig. 3).

An alternative approach would be to assume that the loop-top region acts as a thick target to electrons below some energy,  $E_t$ , following the work of Wheatland & Melrose (1995). Making this assumption we would expect the *inferred* spectral indices from the observed flux ratios, assuming a pure thick or thin target, to be different by between 0 and 2. An inspection of Figure 9 at the flare maximum (17:28:00 UT) shows that the LO/M1 flux ratio yields  $\delta = 3.0 \pm 0.3$  when a thick target is assumed while the M1/M2 flux ratio yields  $\delta = 3.1 \pm 0.3$  when a thin target is assumed. We can thus explain both the observed flux ratios by assuming the loop-top region acts like a thick target to low-energy electrons and a thin target to high-energy electrons with a transition around  $E_t \simeq 20$  keV. The transition energy is indicated by the difference between the LO/M1 and M1/M2 ratios being almost exactly equal to the maximum possible, namely, 2.

If we again assume a direct connectivity between the loop top and the footpoint regions, then the electron spectrum that emerges from the loop top should produce the footpoint emission. Following Wheatland & Melrose (1995), we note that the electrons that have traversed the loop-top region will be modified such that

$$F(E, N_0) = \frac{EF(\sqrt{E^2 + E_t^2})}{\sqrt{E^2 + E_t^2}}, \quad (9)$$

where  $N_0$  is the column depth of the loop-top region and  $E_t^2 = 2KN_0$  (with  $K = 2\pi e^4 \ln \Lambda$ ;  $e$  is the charge on an electron and  $\ln \Lambda$  is the Coulomb logarithm). The lack of observed SXT emission from the loop-top region (Tsuneta et al. 1997) suggests that it has a relatively low average density,  $n_e \sim 10^9 \text{ cm}^{-3}$ , which indicates a total column depth of  $N_0 \simeq n_e l \simeq 10^{18} \text{ cm}^{-2}$  for a source length of  $l \simeq 10^9 \text{ cm}$ . This would result in a transition energy of  $E_t \simeq 2.3$  keV. Our inferred value of  $E_t \simeq 20$  keV therefore would require a column depth of  $N_0 \simeq 10^{20} \text{ cm}^{-2}$ , indicating filling factors  $\simeq 1\%$ . Adopting the higher value for  $E_t$ , we can calculate the modification of the spectrum as expressed in equation (9). The details of this can be found in Wheatland & Melrose (1995). For the present purposes,

however, we need only note that the part of the electron spectrum above  $E = E_t$  effectively “sees” a thin target and will therefore remain unmodified with a spectral index of  $\delta(E > E_t) = 3.1$ . We would then expect the spectral index from the M1/M2 and M2/HI flux ratios at the footpoints to yield a similar value. Figure 10 shows that the inferred electron spectrum at these higher energies is significantly softer than that required to produce the loop-top emission at these energies. The interaction of an electron beam with ambient particles via Coulomb collisions results in a hardening of the spectrum, and so the footpoint and loop-top emission is apparently inconsistent.

In summary, we conclude from the discussion above that a single population of accelerated electrons is unable to reproduce the observed facets of both the loop-top and footpoint emission for the Masuda event.

Neither the inclusion of a cutoff in the electron spectrum at low energies nor the assumption of a loop-top target that is thick to low-energy electrons and thin to high-energy electrons are able to explain the spectral properties of both the loop-top and the footpoint emission. The main problem lies in the fact that the loop-top emission is consistent with a spectrum that is harder than that for the footpoints. The key to this discrepancy may lie in the effects of particle transport and, in particular, in the trapping and precipitation of the accelerated particles. Recently, Aschwanden et al. (1996) have considered such a scenario and have argued for the existence of two distinct particle populations: one which is directly precipitated to the footpoints, yielding *positive* time delays between the emission from high- and low-energy particles; and one which is trapped for a time before being precipitated, yielding *negative* time delays. The evidence for this comes from the temporal analysis of BATSE hard X-ray flare data.

Assuming that the observed negative time delays are a result of particles that were trapped for a time after their initial injection into the corona, Aschwanden et al. (1997) were able to determine the physical nature of the coronal trap. In particular, they found that the delays were consistent with trapping governed by the particle deflection time (i.e., the *weak diffusion limit*; see MacKinnon 1988) with

$$t_{\text{trap}} \sim 0.95 \times 10^8 \left( \frac{E^{3/2}}{n_e} \right) \left( \frac{20}{\ln \Lambda} \right), \quad (10)$$

where  $n_e$  is the electron density,  $\ln \Lambda$  is the Coulomb logarithm, and  $E$  is in units of keV. What is immediately obvious from this expression is that the trapping time is proportional to a positive power of the energy. Consequently, higher energy electrons remain in the trap longer, resulting in a spectrum in the trap that hardens with time. Assuming an injection spectrum of the form  $F(E) = AE^{-\delta}$ , the effect of this spectral hardening on the inferred spectral indices is given by

$$\begin{aligned} \overline{F(E, t)} &= \frac{\int F(E, t) \exp(-t/t_{\text{trap}}) dt}{\int dt} \\ &= \frac{AE^{-\delta} \exp(-\Delta t/t_{\text{trap}}) t_{\text{trap}}}{\Delta t} \\ &\propto E^{-\delta+3/2} \exp \left[ - \left( \frac{\langle E \rangle}{E} \right)^{3/2} \right], \quad (11) \end{aligned}$$

where we have averaged over a trapping time,  $\Delta t = \langle t_{\text{trap}} \rangle = \int F(E)t_{\text{trap}} dE / \int F(E)dE$ .  $\langle E \rangle$  is the average energy associated with the time,  $\Delta t$ , see equation (10), and the exponential is chosen to represent the escape of particles from the trap. Consequently, the average inferred spectrum we would determine from the coronal trap is harder than the injected spectrum by a power of  $\sim 1.5$ . Thus, for an injected spectral index of  $\delta = 4$ , we would expect to measure a trapped spectrum with an index of  $\delta \simeq 2.5$ . This is consistent with the results of Figures 9 and 10 if we also allow the trapped region to act as a thick-thin target of the type described above.<sup>1</sup> In representing the modification to the trapped particle spectrum in this way, we have assumed that the injection of particles is continuous over a time longer than a trapping time. However, this expression also applies to the case of impulsive injection of electrons when the data accumulation time is greater than or equal to the trapping time.

The remaining example, that of an impulsively injected distribution of energetic particles in a low-density trap (where the trapping time is very long), would result in an inferred spectrum that was identical to the injected distribution, since very few particles escape over a single accumulation. In this case, one should observe the gradual hardening of the spectrum as more and more particles escape the trap.

The thermal nature of the Masuda event at late times allows us to determine the density of the loop-top plasma from each of the HXT channels available (LO and M1). A volume of  $\simeq 2 \times 10^{27} \text{ cm}^3$ , corresponding to the bulk of the emission in the integration box covering the loop-top M1 emission (see Fig. 2), is chosen as an upper limit to the volume of the loop-top source. Equations (7) and (8) then enable us to calculate the density from the observed count rates. We find that each channel independently yields the same density (to within less than 5%) and that this density increases from  $2 \times 10^9 \text{ cm}^{-3}$  to  $5 \times 10^9 \text{ cm}^{-3}$  over the period 17:30:00–17:31:20. (Decreasing the volume by a factor of 10, a filling factor of 10% for example, would increase these numbers by approximately a factor of 3.) These values are consistent with electron trapping studies that indicate an energy dependence consistent with collisional electron deflection times (Aschwanden et al. 1997). The densities obtained from the HXT observations give some explanation why only weak SXT emission is seen at this location (Tsuneta et al. 1997). For the volume given above, the emission measure of the hard X-ray emitting plasma in the loop-top source region is at most  $3 \times 10^{46} \text{ cm}^{-3}$ , which for a temperature  $\sim 30 \text{ MK}$  corresponds to an SXT signal of  $\approx 1.4$  counts per pixel in the thin aluminum filter (Al.1) for a typical flare exposure (1 ms). The situation is worse for the thicker filters used to determine temperatures.

Further, we can calculate the conductive and radiative cooling times for the loop-top source given its thermal nature (see Raymond, Cox, & Smith 1976). We find that the conductive cooling time is  $t_{\text{cond}} \approx 0.5 \text{ s}$  and the radiative

cooling time is  $t_{\text{rad}} \approx 5 \times 10^4 \text{ s}$  for the plasma to cool from 40 MK to 20 MK. Observationally, the loop-top source cools on a timescale of order 180 s (see Fig. 9). This would suggest an additional energy input during this period that is borne out by the time development of the density discussed above. There is clearly a mass flow into the loop-top region during this gradual phase. In fact, this influx of mass dominates the energy content of the loop-top region during this time: the thermal energy increases from  $1.6 \times 10^{28}$  to  $3.4 \times 10^{28}$  ergs, despite the fact that the plasma is cooling.

## 7. DISCUSSION AND CONCLUSION

In this paper we have discussed a pixon reconstruction of the flare of 1992 January 13 as observed by the *Yohkoh*/HXT. This flare has received a lot of attention in the solar community because it clearly showed a compact source of hard X-ray emission in the corona that was impulsive in nature. The presence of such a source of emission, while rare, has important implications for models of flare energy release and transport. Indeed, several papers have attempted to explain the enigmatic results first reported by Masuda (1994), for example, Shibata et al. (1995), Fletcher (1995, 1996), Wheatland & Melrose (1995), and Aschwanden et al. (1996). These papers have mostly been of a theoretical nature and relied heavily on the published results of the data analysis (Masuda et al. 1994). In the present work, we have incorporated recent modifications to the HXT reconstruction codes and adopted the pixon approach of Metcalf et al. (1996) to perform a detailed spectral analysis of the Masuda flare. The pixon reconstruction method has a better noise suppression and results in better photometry than MEM. We have also identified the problem of weak source suppression that was inherent to the previous analyses of this event. Consequently, the analysis presented here has improved on and extended that of previous works.

The improved photometry of the pixon approach yields a stronger loop-top source, relative to the footpoint emission, and consequently allows for better temporal and spectroscopic analyses of the distinct sources of emission in this event. We have carried out a more detailed analysis of the loop-top source in this flare than has been previously considered. We also adopted a number of potential distributions of energetic electrons as the source of the observed hard X-ray emission and used the HXT data to constrain the spectral parameters of the selected distribution. Our goal was to find a consistent set of parameters defining the spectral characteristics of the injected electrons, i.e., a single power law or temperature, using the available ratios of the fluxes in the HXT channels. This allowed us to obtain the spectral properties without a knowledge of ambient plasma conditions, such as the density or the source volume.

Using the above approach, we found a remarkably consistent picture with a well-defined temporal evolution of the hard X-ray production. Specifically, we have determined that, in agreement with the MEM results of Masuda (1994), a compact loop-top hard X-ray source exists and that it shows an impulsive behavior during the time of the peak flare emission. However, it has a gradual decay lasting some 5 minutes, during which the loop-top source is thermal in nature. The location of the loop-top source does not change throughout the duration of the event and always lies above the soft X-ray loop (Masuda et al. 1994). It is not clear from the time profile shown in Figure 5 and the spectral evolution shown in Figure 8 whether the thermal source seen late

<sup>1</sup> It is worth noting that a trap with mirror points in the chromosphere (as is typically assumed) would not necessarily produce a localized hard X-ray source in the corona. The coronal emission from the trapped electrons should be distributed uniformly throughout the coronal portion of the loop unless the additional caveat of a population with preferentially large pitch angles was assumed.

in the event is the same as the impulsive source seen during the main phase of the flare. Clearly, there is a thermal development that involves the buildup of the LO channel emission relative to that of the M1 emission at the location of the earlier impulsive source.

The lack of LO channel emission in the loop-top region during the impulsive phase suggests that the loop-top emission is not thermal in nature at that time. A nonthermal description of the particle distribution responsible for the observed hard X-ray production is, we believe, more appropriate. However, the LO channel emission can only be explained by the presence of a low-energy cutoff, with  $E_c \simeq 19$  keV, in the electron distribution and/or a loop-top region with a column depth of  $\approx 10^{20}$  cm<sup>-2</sup> acting as a thick target to electrons below  $E \simeq 20$  keV. In either case, the particle distribution that emerges from the loop-top region is unable to produce the observed characteristics of the footpoint emission, possibly indicating the need for the trapping of electrons in the corona. The thermal phase of the loop top is seen in both the LO and M1 channels of the HXT and is characterized by a peak temperature of 40 MK, immediately following the impulsive nonthermal phase, which decays to  $\sim 20$  MK over the course of some 300 s. The temperatures attained during this thermal phase are consistent with those determined from the Fe xxv channel of the BCS.

The detailed time development of the hard X-ray loop-top source in the Masuda event provides strict requirements for any models purporting to “explain” this observation. In particular, the combination of nonthermal and thermal phases displayed by the M1 channel (23–33 keV) and the lack of any direct connection between the footpoints and loop top during the flare peak present a scenario unlike any of the models put forward to date. As an illustration, the scenario described by Shibata et al. (1995) and Tsuneta et al. (1997), whereby the loop-top source is produced by thermal bremsstrahlung from a 200 MK plasma formed by a fast bow shock resulting from magnetic reconnection at an X-type neutral point, is less appealing in light of the apparent nonthermal nature of this source at the peak of the flare, a result that is supported by the lack of LO channel emission from the loop top.

The in situ production of hard X-ray photons requires a localized energy deposition resulting from the interaction of the energy carrying particles with the ambient medium. Assuming these particles to be electrons accelerated (or heated) by the flare initialization, the region containing the loop-top source has to either have a significant density, have an ultrahigh temperature, or be able to contain the electrons for times comparable to the energy loss time of 20–150 keV electrons. An ambient coronal plasma with a density high enough to thermalize a significant number of electrons of energies greater than 20 keV would be easily detectable by the SXT. However, as discussed in the Introduction, the hard X-ray loop-top source appears to be quite distinct from the flaring loop seen in soft X-rays. A low-density isothermal source has also been ruled out by the analysis presented in this paper since no consistent temperature for the loop-top source was found using the HXT flux ratios. This leaves the trapping of electrons in the source region as the only tenable option.

If electrons are to exist in the loop top long enough to produce the observed signature, then either there has to be a significant number of large pitch angle electrons *and* the

pitch angle scattering has to be extremely low, indicating a very low-density plasma, or the particles have to be injected continuously over a time of order 60–120 s. The latter condition is merely stating that the impulsive signature observed in the photon emission mirrors the temporal behavior of the particle injection. The model of Fletcher (1995) considered the former of these possibilities by invoking the presence of a converging magnetic field. The varying field sets up a loss cone that in turn separates the injected electrons into two distinct populations, one that remains trapped in the corona and one that precipitates to the chromosphere. This agrees in form with the conclusions of Aschwanden et al. (1996) who argue that the bulk of the hard X-ray emission is generated by a population of trapped electrons, while the individual pulses superimposed on the hard X-ray light curve are generated by electrons that precipitate. The arguments presented by Aschwanden et al. (1996) are quite convincing as they use measurements of the direct time of flight of particles from production (in the acceleration region) to thermalization (in the loop footpoints).

The production of a compact source of coronal emission requires more than the trapping of the electrons by the field convergence invoked by Fletcher (1995) and Aschwanden et al. (1996), however. Either a localized field convergence has to occur (e.g., a magnetic pinch; cf. Sakai, Zhao, & Nishikawa 1994), or the electrons have to have pitch angles close to 90 degrees (equivalent to  $v_{\parallel} \simeq 0$ ) causing them to propagate slowly down the legs of the loop. Fletcher (1995) chose an initial electron distribution that was isotropic in pitch angle cosine and consequently was weighted toward higher pitch angles. Typically, the pitch angle scattering is significant at typical coronal densities (Hudson 1972; MacKinnon 1988), and any large pitch angle electron will soon be scattered to a lower pitch angle (higher  $v_{\parallel}$ ) and quickly leave the region of the loop top. The key component missing from Fletcher’s work is the time development. In her model a steady state was assumed, and as a result the emission was integrated over the whole lifetime of the injected particles. Combined with the impulsive injection [ $s(t) = \delta(t - t_0)$ ], this has the effect of producing a loop-top source that is strictly valid only over a few seconds (a typical electron lifetime). An extension of this model to include a time-dependent source function for the particle injection would seem to be a logical next step.

The flare of 1992 January 13 is one of only six discovered by the *Yohkoh*/HXT that exhibited the phenomenon of impulsive coronal hard X-ray sources (Masuda 1994). However, it is clearly an observation of some importance given the implications for the understanding of the flaring process. The results presented here (and previously) show a well-defined temporal evolution that displays many features previously identified in spectroscopic and hydrodynamic modeling studies (e.g., Mariska et al. 1989). However, the impulsive nature of the loop top remains a puzzle. The class of flares to which this belongs may be the exception rather than the rule but an understanding of the processes involved will have a strong influence on flare studies in general.

We would like to thank Professor Takeo Kosugi and Dr. Hugh Hudson for useful discussions. We would also like to acknowledge Dr. William Wagner at NASA for providing travel funding for several participants at the HXT Image

Processing Workshop held at Lockheed Martin Advanced Technology Center, 1997 January 13–16. Finally, we would like to acknowledge the help of the referees (Dr. Markus Aschwanden and Professor Saku Tsuneta) for their insight-

ful comments. *Yohkoh* is a mission of the Japanese Institute for Space and Astronautical Science. This work is supported by NASA under contract NAS 8-37334.

## REFERENCES

- Alexander, D. 1997, Report of HXT Image Reconstruction Workshop, 1997 January 13–16, Lockheed-Martin Palo Alto Research Lab  
 Aschwanden, M. J., Bynum, R. M., Kosugi, T., Hudson, H. S., & Schwartz, R. A. 1997, *ApJ*, 487, 936  
 Aschwanden, M. J., Hudson, H. S., Kosugi, T., & Schwartz, R. A. 1996, *ApJ*, 464, 985  
 Cargill, P., Emslie, A. G., & Simnett, G. M. 1996, *Eos*, 27, 353  
 Duijveman, A., Hoyng, P., & Machado, M. E. 1982, *Sol. Phys.*, 81, 137  
 Feldman, U., Hiei, E., Phillips, K. J. H., Brown, C. M., & Lang, J. 1994, *ApJ*, 421, 843  
 Fletcher, L. 1995, *A&A*, 303, L9  
 ———. 1996, *A&A*, 310, 661  
 Forbes, T. G., & Acton, L. W. 1996, *ApJ*, 459, 330  
 Hoyng, P., et al. 1981, *ApJ*, 244, L153  
 Hudson, H. S. 1972, *Sol. Phys.*, 24, 414  
 Kosugi, T., et al. 1991, *Sol. Phys.*, 136, 17  
 Loredo, T. J. 1990, in *Maximum Entropy and Bayesian Methods*, ed. P. Fougere (Dordrecht: Kluwer), 81  
 MacKinnon, A. L. 1988, *A&A*, 194, 279  
 Mariska, J. T., Emslie, A. G., & Li, P. 1989, *ApJ*, 341, 1067  
 Masuda, S. 1994, Ph.D. thesis, Univ. Tokyo  
 ———. 1997, in *ASP Conf. Ser. 111, Magnetic Reconnection of the Solar Atmosphere*, ed. R. D. Bentley & J. T. Mariska (San Francisco: ASP), 166  
 Masuda, S., et al. 1994, *Nature*, 371, 495  
 ———. 1995, *PASJ*, 47, 677  
 Metcalf, T. R., Alexander, D., & Kosugi, T. 1997, in preparation  
 Metcalf, T. R., Hudson, H. S., Kosugi, T., Puetter, R. C., & Piña, R. K. 1996, *ApJ*, 466, 585  
 Phillips, K. J. H., Bhatia, A. K., Mason, H. E., & Zarro, D. M. 1996, *ApJ*, 466, 549  
 Piña, R. K., & Puetter, R. C. 1993, *PASP*, 105, 630  
 Puetter, R. C. 1995, *Int. J. Image Systems Technol.*, 6, 314  
 Raymond, J. C., Cox, D. P., & Smith, B. W. 1976, *ApJ*, 204, 290  
 Ryan, J. M., & Hudson, H. S. 1995, *ARA&A*, 32, 239  
 Sakai, J. I., Zhao, J., & Nishikawa, K. I. 1994, *Sol. Phys.*, 154, 97  
 Sakao, T. 1994, Ph.D. thesis, Univ. Tokyo  
 Sato, J. 1997, Ph.D. thesis, Graduate Univ. Advanced Studies  
 Shibata, K., et al. 1995, *ApJ*, 451, L83  
 Takakura, T. 1992, *Sol. Phys.*, 142, 327  
 Takakura, T., et al. 1984, *Adv. Space Res.*, 4, No. 7, 143  
 ———. 1993, *PASJ*, 45, 737  
 Tandberg-Hanssen, E., & Emslie, A. G. 1988, *The Physics of Solar Flares* (Cambridge: Cambridge Univ. Press)  
 Tsuneta, S. 1984, Ph.D. thesis, *Ann. Tokyo Astron. Obs.*, 20, 1  
 ———. 1996, in *Solar and Astrophysical Magnetohydrodynamic Flows*, ed. K. Tsinganos (Dordrecht: Kluwer), 85  
 Tsuneta, S., Masuda, S., Kosugi, T., & Sato, J. 1997, *ApJ*, 478, 787  
 Wang, H., et al. 1995, *ApJ*, 444, 115  
 Wheatland, M. S., & Melrose, D. B. 1995, *Sol. Phys.*, 158, 283  
 Willingale, R. 1981, *MNRAS*, 194, 359